

Observation and analysis of defect cluster production and interactions with dislocations

S.J. Zinkle *, Y. Matsukawa

Metals and Ceramics Division, Oak Ridge National Laboratory, P.O. Box 2008, Oak Ridge, TN 37831-6138, USA

Abstract

The current understanding of defect production fundamentals in neutron-irradiated face centered cubic (FCC) and body centered cubic (BCC) metals is briefly reviewed, based primarily on transmission electron microscope observations. Experimental procedures developed by Michio Kiritani and colleagues have been applied to quantify defect cluster size, density, and nature. Differences in defect accumulation behavior of irradiated BCC and FCC metals are discussed. Depending on the defect cluster obstacle strength, either the dispersed barrier hardening model or the Friedel–Kroupa–Hirsch weak barrier model can be used to describe major aspects of radiation hardening. Irradiation at low temperature can cause a change in deformation mode from dislocation cell formation at low doses to twinning or dislocation channeling at higher doses. The detailed interaction between dislocations and defect clusters helps determine the dominant deformation mode. Recent observations of the microstructure created by plastic deformation of quenched and irradiated metals are summarized, including in situ deformation results. Examples of annihilation of stacking fault tetrahedra by gliding dislocations and subsequent formation of mobile superjogs are shown.

© 2004 Elsevier B.V. All rights reserved.

1. Introduction

Professor Michio Kiritani made numerous seminal contributions to our understanding of fundamental aspects of defect production and accumulation in quenched and irradiated metals [1–12]. His unfortunate passing has created a void in the fusion materials research community. He continually displayed innovation in utilizing advanced electron microscopy techniques and intuitive analytical modeling to uncover many of nature's mysteries regarding defect production and accumulation in irradiated metals. Following in his footsteps, this paper briefly reviews the current understanding of defect production fundamentals in several irradiated face centered cubic (FCC) and body centered cubic (BCC) metals in Section 2. Several significant differences between defect accumulation behavior of irradiated BCC and FCC metals, as well as between

different FCC metals, are highlighted. The effect of these radiation-induced defect clusters on hardening behavior is summarized in Section 3. Finally, some fundamental aspects of dislocation interactions with defect clusters are reviewed in Section 4, including recent in situ TEM observations of the interaction and annihilation of stacking fault tetrahedra in quenched gold during room temperature plastic deformation.

2. Defect cluster production

During the early to mid-1980s, Kiritani and co-workers definitively demonstrated the superiority of weak beam electron microscopy for quantitative analysis of small defect clusters produced during neutron irradiation [4,13–15]. Prior to their studies, weak beam microscopy was routinely used by only a few radiation effects researchers [16,17]. The standard electron microscopy method for imaging small defect clusters from the 1960s until the 1980s was based on dynamical two-beam bright field imaging [18–22]. Fig. 1 shows an example of the small defect clusters visible under weak

* Corresponding author. Tel.: +1-865 576 7220; fax: +1-865 241 3650.

E-mail address: zinklesj@ornl.gov (S.J. Zinkle).

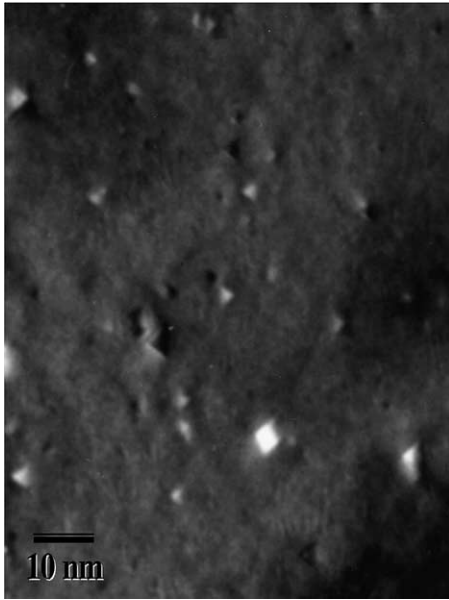


Fig. 1. Weak beam (g , $5g$, $g = 002$) microstructure of copper irradiated with 750 MeV protons to 0.5 dpa at 90 °C [23]. The foil orientation is near the (1 1 0) zone axis.

beam imaging conditions in irradiated bulk copper [23]. Both light- and dark-diffracting defect clusters are visible in this specimen (foil thickness ~ 25 nm), due to depth-dependent variations in diffraction contrast. A variety of defect cluster shapes are visible in this micrograph, which was taken using the (g , $5g$, $g = 002$) weak beam diffraction condition in a foil oriented near the (1 1 0) zone axis. Differentiation between stacking fault tetrahedra (SFTs) and partially dissociated triangle loops requires observation at zone axes $B = 001$ and 110 [24]. For the conditions shown in Fig. 1, about 90% of the visible defect clusters in irradiated copper were identified to be SFTs (visible in Fig. 1 as triangle-shaped defects).

Quantification of small defect clusters is best performed using weak beam electron microscopy in very thin foils. Foil thicknesses of ~ 100 nm commonly used for conventional electron microscopy studies are too thick to accurately observe the small defect clusters produced by low temperature neutron irradiation [18,24]. In particular, imaging of dark-diffracting defects must be performed in very thin (< 40 nm) foil regions; they are not visible in thicker foil regions due to poor contrast with the surrounding matrix. In addition, many of the small bright-diffracting defects are not visible in thicker foil regions. Fig. 2 illustrates the effect of foil thickness on the measured defect cluster size distributions in 14 MeV neutron irradiated copper that was irradiated as bulk specimens [24]. The weak beam imaging conditions (g , $4g$, $g = 002$) and zone axis

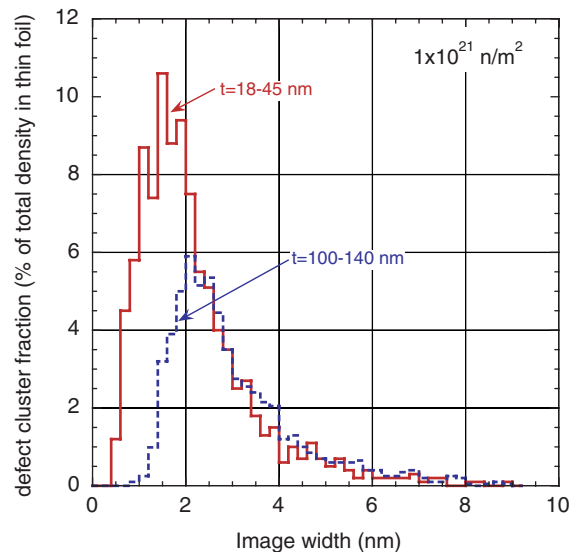


Fig. 2. Effect of foil thickness on the measured defect cluster size distributions in copper irradiated with 14 MeV neutrons at room temperature to a dose of 3.6×10^{-4} dpa [24].

($B = 110$) were held constant for all of the foil thicknesses. Small defect clusters (image sizes below ~ 2 nm) are not easily visible in foils with thicknesses above ~ 40 nm, which causes the apparent size distribution to shift to larger sizes and the apparent density to decrease compared to values measured in very thin regions. The measured defect cluster density in neutron irradiated copper for 'standard' (~ 100 nm) foil thicknesses is nearly a factor of two lower than the value measured in very thin foils. Image simulations performed by Satoh et al. indicate the actual defect cluster size is similar to the observed SFT image size in weak beam microscopy, and that the best visibility is achieved at large deviations from the Bragg condition (e.g. $>g$, $5g$) with a $g = 002$ diffraction vector [25].

For a comprehensive analysis of the microstructure produced in irradiated metals, a wide range of foil thicknesses needs to be examined. Very thin regions (< 40 nm) are used to count SFTs and small defect clusters ($d < 3$ nm), using total magnifications $> 5 \times 10^5$. Larger defect clusters ($d > 3$ nm) and network dislocation density are quantified in thicker foil regions (50–200 nm). In all cases, the possibility of errors due to loss of glissile clusters to the foil surface, annihilation of larger loops due to intersection with the foil surface, or small cluster invisibility due to excessive foil thickness needs to be checked by analyzing the areal cluster density vs. foil thickness, the slope of which gives the volumetric density [26,27]. The plot of areal cluster density vs. foil thickness should linearly extrapolate to the origin. Deviation from linearity is an indication of defect invisibility (due to too

large of foil thickness during observation) or loss of defects by processes such as glide to the foil surface, etc.

Defect clusters are visible in Cu and Ni neutron-irradiated near room temperature at all examined doses [4,28]. The presence of a significant density of visible clusters even at very low doses near $\sim 10^{-5}$ dpa (where the probability of cluster formation from point defect nucleation and growth processes is very small), along with the linear dose accumulation rate of defect cluster density observed at these low doses, implies that these visible defect clusters are produced directly in the displacement cascades in Cu and Ni. For both of these FCC metals, the defect cluster accumulation is initially linear with dose and approaches a constant density at high doses [28]. The nearly constant density at high doses (>0.1 dpa) is due to the destruction of pre-existing defect clusters by new displacement cascades ('cascade overlap' regime) [29,30]. The visible defect cluster density in Cu at low doses is approximately one order of magnitude higher than for Ni [28], implying a higher efficiency for direct in-cascade defect cluster production. This observation of a higher in-cascade defect cluster production efficiency in Cu compared to Ni has also been observed in near-surface ion irradiation studies, although the magnitude of the difference was only a factor of two [21,22]. There are insufficient high dose (>0.1 dpa) neutron irradiation data on Ni to determine whether the difference in cluster density between Cu and Ni is maintained in the cascade overlap dose regime. The higher defect cluster production efficiency for Cu has been attributed to thermal spike effects associated with differences in electron–phonon coupling and melting temperature [22,31,32]. The measured defect cluster size in ion and neutron irradiated copper is nearly constant over a wide range of dose levels (10^{-5} to 40 dpa) for irradiation near room temperature, with a mean value near 2.5 nm [5,24,33,34]. This size independence, along with recent MD simulation results on SFT formation [35–37], provide further evidence that defect clusters (including SFTs) are directly produced in displacement cascades in copper.

It is worth noting that SFTs are the predominant observed defect cluster geometry ($\sim 90\%$ of total visible defect clusters) in ion or neutron irradiated Cu near room temperature for all doses between 10^{-5} and 40 dpa [5,14,23–25,34,38–40]. This implies that interstitial-type defects in irradiated Cu, which according to MD simulations are mainly in the form of small glissile clusters, do not efficiently interact with each other to form larger sessile clusters that are visible by TEM. The visible interstitial loop density in irradiated copper reaches a maximum at doses near 0.01 dpa [23,41]; irradiation of Cu to higher doses causes the creation of a low network dislocation density ($\sim 1 \times 10^{13}/\text{m}^2$), which is about an order of magnitude lower than that observed in Ni and stainless steel [28,42]. The defect cluster geometry in irradiated Ni initially consists predominantly of SFTs at

low doses (<0.01 dpa) and evolves to predominantly dislocation loops at higher doses [39], implying that interstitial-type defect interactions in Ni are more likely than in copper. The physical mechanisms responsible for this difference in behavior are unclear, although specimen purity along with differences in the size distribution and migration behavior of produced defects should be considered.

It has commonly been assumed by numerous authors that the defect cluster density in irradiated metals increases linearly with increasing dose, up to the onset of cascade overlap which causes a saturation in the cluster density [29,43,44]. However, in several pure FCC metals the defect accumulation as measured by electrical resistivity [24,45–48] or TEM [24,49,50] often appears to exhibit an intermediate dose regime where the defect cluster density is proportional to the square root of dose. The defect accumulation behavior was found to be linear at very low doses (<0.0001 dpa, where the probability of uncorrelated point defect recombination is negligible), and proportional to the square root of dose at higher doses. According to simple kinetic models such as the unsaturable trap model [45–47], the critical dose for transition from linear to square root behavior depends on specimen purity. In this model, the transition to square-root accumulation behavior can be delayed up to high doses if impurity trapping of migrating interstitial-type defects is dominant compared to interstitial–interstitial or interstitial–vacancy reactions. Additional systematic work is needed to confirm the presence and to understand the physical mechanisms responsible for this square root fluence-dependent defect cluster accumulation regime.

In contrast to the behavior observed in medium-mass FCC metals such as Cu and Ni, TEM-visible defect clusters are not produced in pure BCC iron at low doses of ~ 0.0001 dpa [41]. This may be attributed to the very low cascade production efficiency of visible defect clusters in irradiated iron [21,51], which in turn may be associated with the more open crystal lattice structure of BCC metals compared to the FCC structure. Direct production of visible vacancy loops by displacement cascades has been observed for high-mass BCC metals like tungsten. The defect clusters visible by TEM in Fe irradiated near room temperature to moderate doses are predominantly interstitial-type loops; most of the vacancy-type defect clusters produced in neutron-irradiated Fe at low doses are not visible. It should be noted that positron annihilation spectroscopy detected a large number density of submicroscopic cavities ($\sim 10^{24}/\text{m}^3$ for doses above 0.001 dpa) in neutron-irradiated iron [41]. These nanoscale cavities are the predominant vacancy-type defect cluster in irradiated Fe. Therefore, the main difference in defect cluster production for pure medium-mass FCC (Cu, Ni) and BCC (Fe) metals is that the vacancy clusters produced directly in displacement

cascades in the FCC metals (SFTs) have sizes and dislocation contrast that are visible by TEM, whereas the vacancy clusters produced in Fe (nanovoids) are too small to be seen by current state-of-the-art TEM. There is also a difference in dominant vacancy cluster morphology for FCC (planar defects) vs. BCC (three-dimensional cavities). For both the FCC and BCC metals, evolution of the interstitial-type defects into cluster sizes that are visible by TEM typically requires doses of ~ 0.001 dpa or higher.

For all FCC and BCC metals, there is a characteristic temperature above which the defect cluster density decreases rapidly. This so-called Stage V recovery temperature is associated with thermal instability of the vacancy clusters originally produced in displacement cascades [30]. In addition to directly contributing to a decrease in the visible density of vacancy-type defect clusters at temperatures above recovery Stage V, the vacancies released from the clusters can also recombine with self-interstitial atoms in interstitial-type clusters and thereby contribute to interstitial cluster shrinkage and annihilation. The vacancies released from the cascade-produced vacancy clusters can also promote void nucleation and growth. The onset of the void swelling regime in FCC metals occurs at temperatures slightly above the Stage V recovery temperature [42,52]. For BCC metals, limited void swelling can occur even at temperatures below recovery Stage V since a significant concentration of nanoscale cavities (as opposed to planar vacancy clusters in FCC metals) are directly formed at low temperatures [53]. Due to the range of vacancy cluster sizes produced in displacement cascades in a given material, a range of Stage V annealing activation energies exist. The value of the observed Stage V temperature also depends on damage rate (annealing time). Typical Stage V annealing temperatures for fission reactor damage rates ($\sim 10^{-7}$ dpa/s) are ~ 200 °C for Cu, ~ 250 °C for austenitic stainless steel, and ~ 300 °C for V-4Cr-4Ti [33]. One consequence of the temperature dependence of the vacancy defect cluster density is that the nature of the predominant planar defect cluster density typically changes from vacancy loops at low temperatures to interstitial loops at high temperatures. For example, Horiki et al. [54] found that $\sim 93\%$ of the planar defect clusters in austenitic stainless steel irradiated to 0.01–0.1 dpa at 80 °C were vacancy-type, whereas $>70\%$ of the planar defect clusters after irradiation at 300 °C were interstitial type.

3. Radiation hardening mechanisms

3.1. Overview of basic radiation hardening models

One of the key technical challenges for fusion reactor structural materials is the radiation hardening and

embrittlement (decreases in tensile ductility and fracture toughness) that occurs in metals irradiated at temperatures below $\sim 0.3 T_M$, where T_M is the melting temperature. The hardening and embrittlement are controlled by interactions between dislocations and defect clusters. As noted in previous reviews of obstacle-controlled strengthening [44,55,56], two approximate dislocation barrier models have historically been used to describe radiation hardening in metals. The dispersed barrier model [57] is based on straightforward geometrical considerations for obstacles intersecting the dislocation glide plane. It is most appropriate for strong obstacles. An alternative hardening relationship was developed by Friedel–Kroupa–Hirsch (FKH) for weak obstacles [58,59], where the effective interparticle spacing is increased compared to the planar geometric spacing due to less extensive dislocation bowing prior to obstacle breakaway. Using the simple approximation for dislocation line tension $T = \mu b^2/2$, the functional dependence of polycrystalline yield strength increase ($\Delta\sigma$) on defect cluster size and density for these two limiting cases is given by the following equations:

$$\Delta\sigma = M\alpha\mu b\sqrt{Nd}, \quad (1)$$

$$\Delta\sigma = \frac{1}{8}M\mu b d N^{2/3}, \quad (2)$$

where M is the Taylor factor (3.06 for equiaxed BCC and FCC metals), α is the defect cluster barrier strength, μ is the shear modulus, b is the Burgers vector of the primary glide dislocations, and N and d are the defect cluster density and diameter. Although most radiation hardening studies have used the dispersed barrier model (Eq. (1)) for data interpretation, the FKH model (Eq. (2)) may be more appropriate for many radiation-induced small defect clusters which are weak obstacles to dislocation motion. According to some early analyses [55], the FKH model is adequate for barrier strengths up to 1/4 of the Orowan (impenetrable obstacle) limit, i.e., $\alpha < 0.25$. The dispersed barrier model is more appropriate for barrier strengths of $\alpha = 0.25$ –1. Typical experimental values of the defect cluster barrier strength for copper and austenitic stainless steel neutron-irradiated and tested near room temperature are $\alpha = 0.15$ –0.2 [50]. The reported barrier strengths for the visible defect clusters in neutron irradiated V-4Cr-4Ti [60] and other BCC metals [55] are $\alpha = 0.4$ or higher. It is possible that hardening from submicroscopic nanovoids in the BCC metals might cause an overestimation of the reported barrier strength for the visible defect clusters.

Fig. 3 summarizes the dose-dependent shear strength in single crystal copper following fission neutron irradiation and tensile testing near 300 K, as reported by Blewitt et al. [61]. The top figure (Fig. 3(a)) demonstrates that the hardening is approximately linear with the 1/3

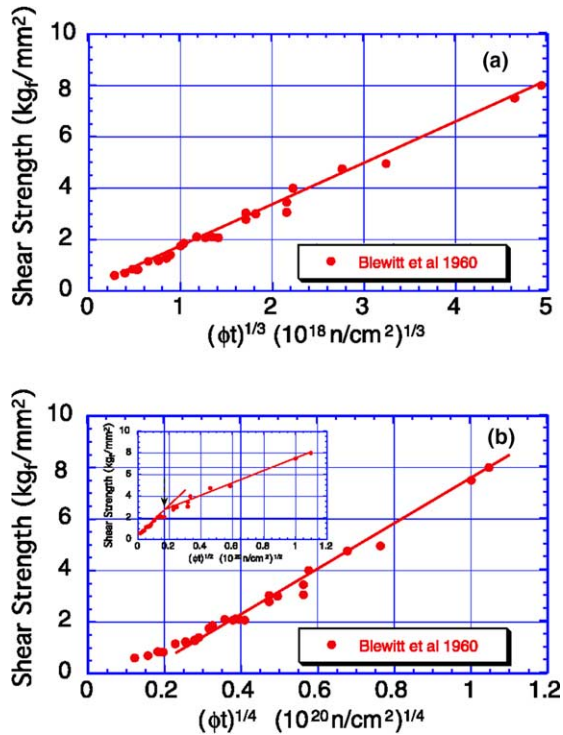


Fig. 3. Dose dependence of radiation hardening in neutron irradiated single crystal copper [61] plotted vs. the (a) one-third and (b) one-fourth power of neutron fluence. The inset figure (a) shows the one-half power dose dependence.

power of fluence for fluences from 10^{16} to 10^{20} n/cm². This 1/3 power dependence reported by Blewitt et al. was criticized by several authors as nonphysical, and a 1/2 power dependence on dose was claimed to be the expected physical relationship [44,62]. A square root dose dependence of radiation hardening would arise from the dispersed barrier hardening model (Eq. (1)) if the defect cluster density increased in direct proportion to dose and the defect size was independent of dose. However, as shown in the inset portion of Fig. 3(b), the shear strength of copper in the experiments by Blewitt et al. is proportional to the square root of fluence only for fluences below 3×10^{18} n/cm². Deviation from the square root hardening behavior occurs at too low of dose ($\sim 3 \times 10^{-4}$ dpa) to be attributable to displacement cascade overlap effects. One possible rationalization of the observed behavior in Fig. 3(b) is to assume dispersed barrier hardening (Eq. (1)), and that the defect cluster accumulation rate in copper changes from linear to a square root dependence at a fluence of $\sim 3 \times 10^{18}$ n/cm². Such a transition in defect cluster accumulation has been observed at similar doses in TEM and electrical resistivity studies of neutron irradiated copper [24]. Alternatively, the 1/3 power dose-dependent hardening behavior shown in Fig. 3(a) could be rationalized based

on the FKH weak barrier hardening model (Eq. (2)) with an extended square root defect cluster accumulation regime. This simple example demonstrates the difficulty to experimentally differentiate between the FKH and dispersed barrier hardening models on the basis of hardening data alone, even for the ~ 4 orders of magnitude range of dose in the study by Blewitt et al. [61]. Microstructural data on these neutron-irradiated specimens would have been very valuable for an unambiguous resolution of this long-standing issue regarding the most appropriate hardening model.

There is a clear need to develop improved radiation hardening models which build upon the physically sound, albeit simplistic, foundations developed over 40 years ago in the dispersed barrier and FKH models. Some examples of required improvements were summarized 25 years ago by Kocks [56]. There has been some limited recent work to improve the dislocation obstacle superposition rules for irradiated metals containing a variety of obstacle strengths [63] and an alternative cascade induced source hardening model has been proposed for irradiated metals [64], but further advances are needed.

3.2. Deformation mechanisms in irradiated metals

It is well established that the dominant deformation mode in BCC and FCC metals irradiated at low temperatures ($< 0.3 T_M$) is dependent on dose [65,66], strain level [65,66] and temperature [66–69]. The formation of cleared dislocation channels is favored at high doses and low strains, whereas dislocation cell formation is favored at low doses and high strains. Twinning is favored in low stacking fault energy materials such as austenitic stainless steel at low temperatures, high strains, and high strain rates. According to calculated Ashby deformation maps for several irradiated FCC and BCC metals [69], twinning appears when glide dislocations are strongly pinned by defect clusters (so that normal dislocation glide deformation cannot occur up to very high stress levels). Dislocation channeling can be considered as a specialized subset of dislocation glide deformation mechanisms [69].

At low strains (less than a few percent), the work hardening rate of metals irradiated at low temperatures is often dramatically reduced compared to unirradiated values. This causes localized necking to occur after low amounts of strain. However, the strain hardenability of irradiated polycrystalline metals becomes similar to the unirradiated case at large plastic strains [70,71]. This may be rationalized as follows. At low amounts of deformation ($< 5\%$ in single crystals), widely separated dislocation channels are created parallel to the primary and cross slip planes. At higher levels of deformation, strain hardening is restored due to activation of additional slip systems. The additional slip systems become

activated due to a multiaxial stress state associated with crystal twisting from the deformation, and from dislocation multiplication arising from interactions between intersecting dislocation channels. These new slip systems promote dislocation network interaction and dislocation multiplication.

4. Dislocation interactions with defect clusters

The coarse slip associated with inhomogeneous ‘jerky’ Stage I flow during deformation of irradiated single crystals has been clearly linked to the formation of cleared dislocation channels [72–74]. The inhomogeneous slip bands form within time periods of <1 ms during tensile deformation. Since these discrete slip bands enable substantial plastic deformation to occur (localized shear strains per channel of 100–700%) [55,73] without the usual dislocation–dislocation interactions that lead to dislocation multiplication and work hardening, dislocation channeling has been widely attributed to be

responsible for the observed low work hardening rates in irradiated metals. One of the key steps in the formation of cleared dislocation channels is removal of clusters by glide dislocations. Therefore, there is considerable interest in understanding the physical mechanisms responsible for the elimination by moving dislocations of vacancy clusters such as SFTs and vacancy loops. Both computational simulations [75–79] and in situ TEM observations during straining [76,80] are being utilized. Continued advances in electron microscopy tools and computational simulations have enabled similar size scales to be examined via experiment and modeling. However, a large difference in accessible time scales for MD (~1 ns) and in situ electron microscopy (<1 ms) still exists. Several questions have recently been raised regarding the SFT annihilation process, namely whether annihilation of a ‘perfect’ (non-truncated) SFT can occur (SFTs produced by neutron irradiation might be imperfectly formed due to the ~10 ps rapid quench in displacement cascades) and whether annihilation requires defect cluster interaction with multiple gliding dislocations.

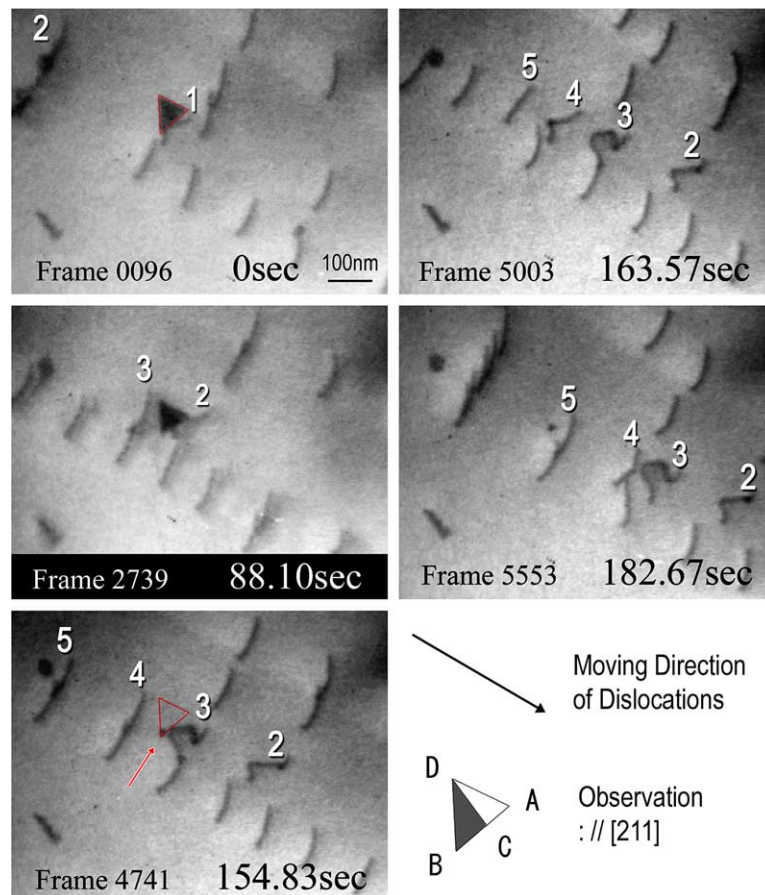


Fig. 4. SFT annihilation and superjog formation and migration in quenched gold. The elapsed time is given in the lower right hand region of each panel. The inset white numbers identify the sequence of dislocations impinging on the SFT.

Fig. 4 shows a series of images from an in situ TEM video investigation of dislocation interactions at room temperature with SFTs in a quenched gold specimen [80]. The first and second gliding dislocations interact with the SFT without causing annihilation. Nearly complete destruction of the SFT occurred while the third dislocation was in direct physical contact. A small remnant SFT corresponding to the original peak of the SFT remained following the annihilation, and a superjog was created on the interacting dislocation. Upon further straining, the superjogged-dislocation displayed significant mobility.

Fig. 5 shows an example of annihilation of a large (perfectly formed) SFT in quenched gold by a single dislocation during in situ TEM deformation at room temperature [80]. A band of dislocations was originally pinned by the SFT. After several seconds of physical contact, the leading dislocation annihilated the SFT. A small remnant SFT corresponding to one of the tips of the original SFT was observed following the annihilation, whereas the rest of the SFT disappeared. In this SFT-dislocation interaction, the dislocation that caused the SFT annihilation was observed to cross-slip immediately after the SFT was destroyed, and then cross-slipped onto a glide plane parallel to the original slip plane.

Numerous aspects of the detailed physical mechanism(s) involved in defect cluster annihilation still need to be elucidated [33], including examination of the role of dislocation reactions vs. vacancy absorption, whether or not the SFT collapses to a planar loop as an intermediate step in the annihilation process, the importance of vacancy pipe diffusion along the gliding dislocation core for defect cluster annihilation, and the effect of experimental variables such as strain rate, dislocation velocity, test temperature, and applied stress. Recent molecular dynamics simulations indicate the dislocation barrier stress of SFTs decreases with increasing glide plane distance from the base of the SFT [33,79]. There is also preliminary evidence that the SFT annihilation probability during dislocation interactions may decrease with decreasing defect cluster size and increasing density [80]. Relatively little work has been performed to date comparing annihilation mechanisms by gliding dislocations for SFTs vs. vacancy loops.

5. Conclusions

Microstructural investigations are a key tool for fundamental understanding of defect accumulation and

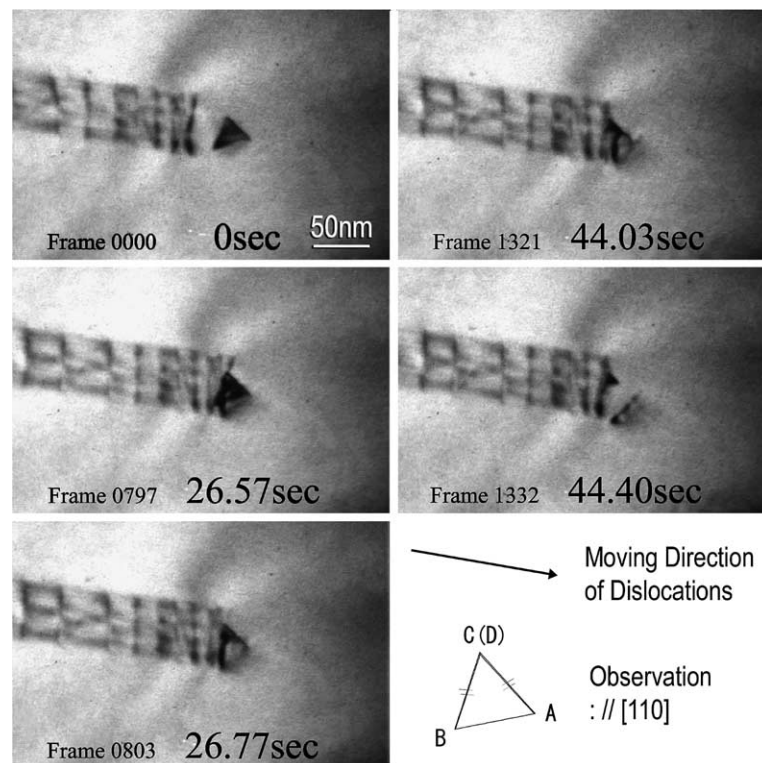


Fig. 5. SFT annihilation by a single dislocation in quenched gold. The elapsed time is given in the lower right hand region of each panel.

defect cluster–dislocation interactions in fast neutron-irradiated materials. Visible vacancy-type defect clusters are formed directly in fission neutron displacement cascades in medium-mass FCC metals such as Cu and Ni, whereas TEM-visible defect clusters are not directly formed in medium-mass BCC metals such as Fe. With increasing dose and temperature, the dominant planar defect cluster morphology in Ni and stainless steel changes from vacancy-type SFTs and dislocation loops to interstitial-type loops. In the case of pure copper, the SFT remains the dominant visible defect cluster geometry over a wide range of doses and temperatures. The physical mechanisms responsible for this difference in behavior between Cu and Ni are not yet resolved; specimen purity and displacement cascade thermal spike effects may be playing a role. Whereas planar defect clusters (SFTs or loops) are the dominant vacancy cluster geometry in irradiated FCC metals at temperatures below recovery Stage V, nanoscale voids appear to be the dominant geometry in many irradiated BCC metals including Fe. Further work is needed to determine the effect of impurities and other experimental variables on the preferred defect cluster morphology and dose dependence of defect accumulation during irradiation.

Relatively little has occurred in the development of radiation hardening models over the past 40 years. General trends associated with radiation hardening are still being analyzed using the physically sound but simplistic dispersed barrier and Friedel–Kroupa–Hirsch weak barrier models. Further improvements in these simplistic models are needed to describe the hardening in typical irradiated metals that have a variety of obstacles present.

Neutron irradiation at temperatures below recovery Stage V can cause significant changes in the deformation mode of metals. Dislocation channeling is of particular interest, since it may enhance flow localization. Dislocation interactions with radiation-induced defect clusters are a key link for understanding the deformation behavior of irradiated metals. In particular, the physical mechanisms that cause annihilation of defect clusters need to be determined. Recent *in situ* TEM deformation studies on quenched gold specimens have clearly demonstrated that large ideally formed SFTs can be annihilated by even a single gliding dislocation. The effects of numerous experimental variables including test temperature, strain rate, dislocation velocity, applied stress, and cluster size and density need further investigation.

Acknowledgements

The authors are deeply indebted to the late Professor Michio Kiritani for inspiring their research efforts. We also thank Yuri Osetsky, Stas Golubov, Roger Stoller

and Bachu Singh for stimulating discussions on the topics described in this paper. This work was sponsored by the Office of Fusion Energy Sciences, U.S. Department of Energy under contract DE-AC05-00OR22725 with UT-Battelle, LLC.

References

- [1] S. Yoshida, M. Kiritani, Y. Shimomura, in: R.M.J. Cotterill et al. (Eds.), *Lattice Defects in Quenched Metals*, Academic, New York, 1965, p. 713.
- [2] S. Yoshida, M. Kiritani, Y. Deguchi, N. Kamigaki, *Trans. JIM* 9 Supplement (Proc. ICSMA-1) (1968) 83.
- [3] M. Kiritani, in: M.T. Robinson, F.W. Young Jr. (Eds.), *Fundamental Aspects of Radiation Damage in Metals*, vol. II, CONF-751006-P2, National Tech. Inform. Service, Springfield, VA, 1975, p. 695.
- [4] M. Kiritani, *J. Nucl. Mater.* 137 (1986) 261.
- [5] M. Kiritani, *J. Nucl. Mater.* 155–157 (1988) 113.
- [6] M. Kiritani, *J. Nucl. Mater.* 169 (1989) 89.
- [7] M. Kiritani, T. Yoshiie, S. Kojima, Y. Satoh, *Radiat. Eff. Def. Solids* 113 (1990) 75.
- [8] M. Kiritani, T. Yoshiie, S. Kojima, Y. Satoh, K. Hamada, *J. Nucl. Mater.* 174 (1990) 327.
- [9] M. Kiritani et al., *J. Nucl. Mater.* 212–215 (1994) 192.
- [10] M. Kiritani et al., *J. Nucl. Mater.* 212–215 (1994) 241.
- [11] Y. Kizuka, Y. Satoh, S. Arai, M. Kiritani, *Radiat. Eff. Def. Solids* 145 (1998) 143.
- [12] M. Horiki, M. Kiritani, *J. Nucl. Mater.* 239 (1996) 34.
- [13] M. Kiritani, N. Yoshida, S. Ishino, *J. Nucl. Mater.* 122&123 (1984) 602.
- [14] N. Yoshida, Y. Akashi, K. Kitajima, M. Kiritani, *J. Nucl. Mater.* 133&134 (1985) 405.
- [15] M. Kiritani, T. Yoshiie, S. Kojima, *J. Nucl. Mater.* 141–143 (1986) 625.
- [16] H.R. Brager, F.A. Garner, N.F. Panayotou, *J. Nucl. Mater.* 103&104 (1981) 955.
- [17] M.L. Jenkins, D.J.H. Cockayne, M.J. Whelan, *J. Microsc.* 98 (Part 2) (1973) 155.
- [18] M. Rühle, J.C. Crump III, *Phys. Stat. Sol. (a)* 2 (1970) 257.
- [19] B.L. Eyre, *J. Phys. F* 3 (1973) 422.
- [20] C.A. English, *J. Nucl. Mater.* 108&109 (1982) 104.
- [21] M.A. Kirk, I.M. Robertson, M.L. Jenkins, C.A. English, T.J. Black, J.S. Vetrano, *J. Nucl. Mater.* 149 (1987) 21.
- [22] M.L. Jenkins, M.A. Kirk, W.J. Phythian, *J. Nucl. Mater.* 205 (1993) 16.
- [23] S.J. Zinkle, A. Horsewell, B.N. Singh, W.F. Sommer, *J. Nucl. Mater.* 212–215 (1994) 132.
- [24] S.J. Zinkle, *J. Nucl. Mater.* 150 (1987) 140.
- [25] Y. Satoh, H. Taoka, S. Kojima, T. Yoshiie, M. Kiritani, *Philos. Mag. A* 70 (1994) 869.
- [26] N. Yoshida, M. Kiritani, F.E. Fujita, *J. Phys. Soc. Jpn.* 39 (1975) 170.
- [27] S. Kojima, S.J. Zinkle, H.L. Heinisch, *J. Nucl. Mater.* 179–181 (1991) 982.
- [28] B.N. Singh, S.J. Zinkle, *J. Nucl. Mater.* 206 (1993) 212.
- [29] A.D. Whapham, M.J. Makin, *Philos. Mag.* 5 (1960) 237.
- [30] S.J. Zinkle, B.N. Singh, *J. Nucl. Mater.* 199 (1993) 173.
- [31] T. Diaz de la Rubia, R.S. Averback, H. Hsieh, R. Benedek, *J. Mater. Res.* 4 (1989) 579.

- [32] I.M. Robertson, D.K. Tappin, M.A. Kirk, *Philos. Mag. A* 68 (1993) 843.
- [33] S.J. Zinkle, N. Hashimoto, Y. Matsukawa, R.E. Stoller, Y.N. Osetsky, in: L.M. Wang et al. (Eds.), *Radiation Effects and Ion Beam Processing of Materials*, MRS Symposium Proceedings, vol. 792, Materials Research Society, Warrendale, PA, 2004, p. R1.1.1.
- [34] S.J. Zinkle, B.N. Singh, *J. Nucl. Mater.* 283–287 (2000) 306.
- [35] Y.N. Osetsky, D.J. Bacon, *Nucl. Instrum. and Meth. B* 180 (2001) 85.
- [36] K. Nordlund, F. Gao, *Appl. Phys. Lett.* 74 (1999) 2720.
- [37] B.D. Wirth, V. Bulatov, T. Diaz de la Rubia, *J. Nucl. Mater.* 283–287 (2000) 773.
- [38] S.J. Zinkle, K. Farrell, *J. Nucl. Mater.* 168 (1989) 262.
- [39] S.J. Zinkle, L.L. Snead, *J. Nucl. Mater.* 225 (1995) 132.
- [40] M. Victoria et al., *J. Nucl. Mater.* 276 (2000) 114.
- [41] M. Eldrup, B.N. Singh, S.J. Zinkle, T.S. Byun, K. Farrell, *J. Nucl. Mater.* 307–311 (2002) 912.
- [42] S.J. Zinkle, P.J. Maziasz, R.E. Stoller, *J. Nucl. Mater.* 206 (1993) 266.
- [43] M.J. Makin, A.D. Whapham, F.J. Minter, *Philos. Mag.* 7 (1962) 285.
- [44] T.J. Koppenaal, R.J. Arsenault, *Metall. Rev.* 16 (1971) 175.
- [45] R.M. Walker, in: D.S. Billington (Ed.), *Radiation Damage in Solids*, Academic, New York, 1962, p. 594.
- [46] L.J. Thompson, G. Youngblood, A. Sosin, *Radiat. Eff.* 20 (1973) 111.
- [47] U. Theis, H. Wollenberger, *J. Nucl. Mater.* 88 (1980) 121.
- [48] S.J. Zinkle, *J. Phys. F: Met. Phys.* 18 (1988) 377.
- [49] T. Muroga, H.L. Heinisch, W.F. Sommer, P.D. Ferguson, *J. Nucl. Mater.* 191–194 (1992) 1150.
- [50] S.J. Zinkle, *Radiat. Eff. Def. Solids* 148 (1999) 447.
- [51] C.A. English, M.L. Jenkins, *Mater. Sci. Forum.* 15–18 (1987) 1003.
- [52] S.J. Zinkle, K. Farrell, H. Kanazawa, *J. Nucl. Mater.* 168 (1991) 262.
- [53] B.N. Singh, J.H. Evans, *J. Nucl. Mater.* 226 (1995) 277.
- [54] M. Horiki, S. Arai, Y. Satoh, M. Kiritani, *J. Nucl. Mater.* 255 (1998) 165.
- [55] A.L. Bement Jr., in: W.C. Leslie (Ed.), *Second International Conference on Strength of Metals and Alloys*, vol. II, American Society for Metals, Metals Park, OH, 1970, p. 693.
- [56] U.F. Kocks, *Mater. Sci. Eng.* 27 (1977) 291.
- [57] A.K. Seeger, in: *Second UN Conference on Peaceful Uses of Atomic Energy*, vol. 6, United Nations, New York, 1958, p. 250.
- [58] J. Friedel, *Dislocations*, Pergamon, New York, 1964.
- [59] F. Kroupa, P.B. Hirsch, *Disc. Faraday Soc.* 38 (1964) 49.
- [60] P.M. Rice, S.J. Zinkle, *J. Nucl. Mater.* 258–263 (1998) 1414.
- [61] T.H. Blewitt, R.R. Coltman, R.E. Jamison, J.K. Redman, *J. Nucl. Mater.* 2 (1960) 277.
- [62] J. Diehl, G.P. Seidel, in: *Radiation Damage in Reactor Materials*, vol. I, IAEA, Vienna, 1969, p. 187.
- [63] G.R. Odette, G.E. Lucas, G. Tedeski, B.D. Wirth, in: *Fusion Materials Semiann. Prog. Rep. for period ending 31 December 1998*, DOE/ER-0313/25, Oak Ridge National Lab., 1998, p. 221.
- [64] B.N. Singh, N.M. Ghoniem, H. Trinkaus, *J. Nucl. Mater.* 307–311 (2002) 159.
- [65] A. Okada, K. Kanao, T. Yoshiie, S. Kojima, *Mater. Trans. JIM* 30 (1989) 265.
- [66] K. Farrell, T.S. Byun, N. Hashimoto, Oak Ridge National Lab., Oak Ridge, TN Report ORNL/TM-2002/63, 2003.
- [67] J.L. Brimhall, J.I. Cole, J.S. Vetrano, S.M. Bruemmer, in: I.M. Robertson et al. (Eds.), *Microstructure of Irradiated Materials*, MRS Symposium Proceedings, vol. 373, Materials Research Society, Pittsburgh, 1995, p. 177.
- [68] N. Hashimoto, S.J. Zinkle, A.F. Rowcliffe, J.P. Robertson, S. Jitsukawa, *J. Nucl. Mater.* 283–287 (2000) 528.
- [69] S.J. Zinkle, G.E. Lucas, in: *Fusion Materials Semiannual Progress Report for Period ending June 30, 2003*, DOE/ER-0313/34, Oak Ridge National Lab., 2003, p. 101.
- [70] S.M. Ohr, *Mater. Res. Bull.* 2 (1968) 213.
- [71] T.S. Byun, K. Farrell, *Acta Mater.* 52 (2004) 1597.
- [72] J.V. Sharp, *Philos. Mag.* 16 (1967) 77.
- [73] J.V. Sharp, *Radiat. Eff.* 14 (1972) 71.
- [74] M.S. Wechsler, R.P. Tucker, R. Bode, *Acta Metall.* 17 (1969) 544.
- [75] B.D. Wirth, V. Bulatov, T. Diaz de la Rubia, *J. Eng. Mater. Technol.* 124 (2002) 329.
- [76] J.S. Robach, I.M. Robertson, B.D. Wirth, A. Arsenlis, *Philos. Mag.* 83 (2003) 955.
- [77] M. Hiratani, H.M. Zbib, B.D. Wirth, *Philos. Mag. A* 82 (2002) 2709.
- [78] Y.N. Osetsky, D.J. Bacon, F. Gao, A. Serra, B.N. Singh, *J. Nucl. Mater.* 283–287 (2000) 784.
- [79] Y.N. Osetsky, R.E. Stoller, Y. Matsukawa, *Proceedings of 11th International Conference on Fusion Reactor Materials*, Kyoto, 7–11 December 2003, *J. Nucl. Mater.*, in press. doi:10.1016/j.jnucmat.2004.04.257.
- [80] Y. Matsukawa, S.J. Zinkle, *Proc. 11th International Conference on Fusion Reactor Materials*, Kyoto, 7–11 December 2003, *J. Nucl. Mater.*, in press. doi:10.1016/j.jnucmat.2004.04.069.